3-2002

Collisional Dynamics of Bi_2 $A(0_u^+)$. II. State-to-state Rotational Energy Transfer

Robert E. Franklin
Air Force Institute of Technology

Glen P. Perram
Air Force Institute of Technology

Recommended Citation

Robert E. Franklin, Glen P. Perram; Collisional dynamics of Bi2 A(0+u). II. State-to-state rotational energy transfer. J. Chem. Phys. 22 March 2002; 116 (12): 4896–4900. https://doi.org/10.1063/1.1451058

The Journal of Chemical Physics

RESEARCH ARTICLE | MARCH 22 2002

Collisional dynamics of Bi_2 $A(0_u^+)$. II. State-to-state rotational energy transfer

Robert E. Franklin; Glen P. Perram

J. Chem. Phys. 116, 4896–4900 (2002)
https://doi.org/10.1063/1.1451058

Collisional dynamics of Bi_2 $A(0_u^+)$. II. State-to-state rotational energy transfer

Robert E. Franklin[a] and Glen P. Perram[b]
Department of Engineering Physics, Air Force Institute of Technology, Wright-Patterson Air Force Base, Ohio 45433-7765

(Received 1 October 2001; accepted 27 December 2001)

Rotational-to-translational $(R-T)$ energy transfer within $v'=1$ of the $A(0_u^+)$ state of Bi_2 has been investigated using spectrally resolved, laser induced fluorescence techniques. Spectrally resolved emissions from collisionally populated rotational levels of $Bi_2(A,v'=1)$ were observed for helium, neon, and argon collision partners after laser excitation of the high rotational levels $J'=171$, 201, and 231. Total rotational removal rates from the initially prepared state range from $2.8-8.9\times10^{-10}$ cm^3/molecule s. Collisional population of rotational states with $|\Delta J|\leqslant 56$ was observed at pressures of 0.09–1.4 Torr. The state-to-state rates are adequately modeled by the energy based statistical power gap law. © *2002 American Institute of Physics.* [DOI: 10.1063/1.1451058]

I. INTRODUCTION

Rotationally inelastic collisions have been studied on a state-to-state basis using laser induced fluorescence techniques, by examining the rotational dependence of pressure broadening coefficients, and from a theoretical basis.[1–8] A variety of energy based and angular momentum based scaling laws have been developed to represent the available data.[1,2] The bismuth dimer offers a unique opportunity to evaluate these scaling laws under conditions of high angular momentum and small energy spacing. The very low rotational constant for Bi_2 offers significant populations in rotational states above $J=200$ even at modest temperatures ($T\approx300$ K). Furthermore, the Bi_2-He collision is highly impulsive.[9] In the present study we examine the state-to-state rotational energy transfer within the Bi_2 $A(0_u^+)v'=1$ state for initially prepared rotational states $J'=171$, 201, 231 and helium, neon, and argon collision partners.

The spectroscopy of the Bi_2 $A(0_u^+)-X(0_g^+)$ system is well characterized, particularly for the low lying vibrational levels.[10–12] However, the collisional dynamics of the $Bi_2(A)$ is less studied. The radiative rates,[13–15] quenching from a few (v',J') levels,[14] and vibrational energy transfer in the lowest vibrational levels[9] have previously been reported. In addition, several $Bi_2(A-X)$ lasers have been demonstrated.[16,17] However, no rotational energy transfer studies have previously been reported.

II. EXPERIMENT

The steady-state laser induced fluorescence apparatus has been described in detail previously.[9] Briefly, a Coherent model 899-29 ring dye laser with rhodamine 590 dye was used to selectively excite the (v',J') levels of the $A(0_u^+)$ state at the frequencies indicated in Table I. The ring dye laser provided sufficient resolution (Doppler limited at about 0.01 cm^{-1}) to prepare a pure rotational state within $Bi_2(A,v'=1)$ for $J>15$. The rotational assignment and spectroscopic constants have previously been reported.[11] A McPherson 1.3 m monochromator with a Princeton Instruments model 1024 SR/B optical multichannel analyzer (OMA) was used to resolve the laser induced fluorescence with a resolution of 0.5 cm^{-1} and a bandwidth of 225 cm^{-1}. The bismuth dimer was generated by heating a small sample of granular bismuth in a 1 cm aluminum oxide crucible and tungsten basket heater to 900–1000 K. The fluorescence chamber was evacuated to less than 0.01 m Torr by an oil diffusion pump and 0.07–1.4 Torr of rare gas (99.996%) was added to induce rotational transfer. The cell pressure was monitored with an MKS model 390×10 Torr capacitance manometer. The spectral response of the OMA was calibrated with a blackbody source at 1266 K.[18]

III. RESULTS

The spectrally resolved emission from the $v'=1\rightarrow v''=5$ band after excitation of $v'=1$, $J'=171$ in the presence of 0.855 Torr of helium is shown in Fig. 1. The strong $P-R$ doublet emission from the laser populated state is clearly evident. The weaker satellite transitions are from the collisionally populated rotational states. Emission is observed only from even rotational levels because the nuclear spin is not readily altered by collisions.[19] For $J'<140$, a near coincidence of the $P(J)$ and $R(J+14)$ lines precludes complete spectral isolation. The rotational transfer rates are quite rapid, with significant population in the satellite states even at low buffer gas pressures.

To extract the populations of the various satellite rotational levels relative to the laser pumped state, a synthetic spectra was modeled and fit to the observed data. The instrumental line shape was analyzed by observing the $2p^5(^2P_{3/2})3s(1_2^0)-2p^5(^2P_{1/2})3p(8_2)$ atomic neon line near 16 821 cm^{-1} in emission from a small discharge lamp, as shown in Fig. 2. A Gaussian–Lorentzian sum of the functional form

[a]Present address: Aeronautical Systems Center, Wright-Patterson Air Force Base, OH 45433.
[b]Electronic mail: glen.perram@afit.edu

TABLE I. Laser excitation frequencies used to prepare vibrational and rotational states.

v_0', v_0''	J_0', J_0''	$\nu(\mathrm{cm}^{-1})$
1, 3	171, 170	17 256.066
1, 3	201, 200	17 222.215
1, 3	231, 230	17 185.199

$$g(\lambda)=2a_0\left\{\frac{\kappa\sqrt{\ln 2}}{R\sqrt{\pi}}\exp\left[-4\ln 2\left(\frac{\lambda-\lambda_0}{R}\right)^2\right]+\frac{1-\kappa}{\pi R\left[1+4\left(\frac{\lambda-\lambda_0}{R}\right)^2\right]}\right\}, \quad (1)$$

where

λ_0=transition line center,
R=spectral resolution (full width at half maximum),
κ=fractional Gaussian nature ($\kappa=0$ for pure Lorentzian, $\kappa=1$ for pure Gaussian),
a_0=intensity scale parameter

is adequate to represent the instrumental line shape. The instrumental linewidth is an order of magnitude larger than the atomic transition linewidth. The instrumental line shape has a significant intensity in the wings due to stray light and aberrations, and is better represented by the sum of Lorentzian and Gaussian profiles than a Voigt profile. The intensity of the neon line emission in Fig. 2 is similar to that for bismuth laser induced fluorescence and is significantly below detector saturation. A computed rotational spectrum is composed by summing a series of common (R,κ) line shapes for each of the *P*- and *R*-branch transitions and using the amplitudes, $a_0(J)$ as the fit parameters. The resolution and fractional Gaussian nature were constrained to the values reported in Fig. 2. The rotational line strengths for these high rotational levels vary by less than 0.3% and the intensities of the *P*- and *R*-branch lines originating from the same emitting rotational level are constrained to yield the same populations. A least-squares fit was achieved with Jandell's PeakFit software and a comparison of the observed and modeled spectra corresponding to a segment of Fig. 1 is shown in Fig. 3.

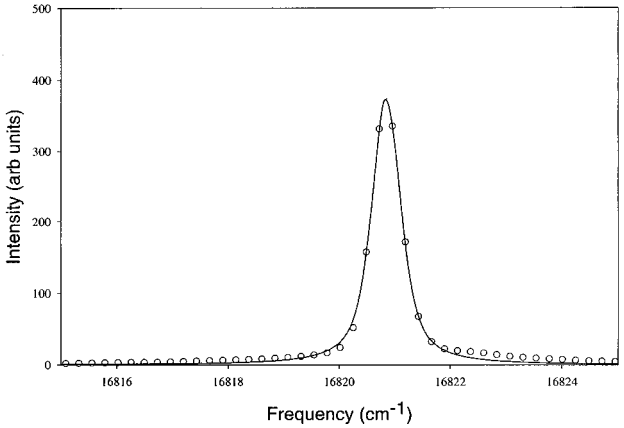

FIG. 2. Monochromator resolution response to neon emission line: (○) observed intensity, (—) fit to Eq. (1) yielding $a_0=3.77\pm0.04\times10^5$, $v_0=1/\lambda_0=16\,820.846\pm0.003\ \mathrm{cm}^{-1}$, $R=0.623\pm0.01\ \mathrm{cm}^{-1}$, and $\kappa=0.25\pm0.04$.

A plot of the population in the satellite level $J'=165$ relative to the population in the parent level, $J'=171$, is shown as a function of helium buffer gas pressure in Fig. 4. The error bounds indicated in Fig. 4 are obtained from the uncertainties in the amplitudes from the spectral fits. Similar data were obtained for initially pumped states $J_0'=171$, 201, and 231 and satellite states $-56<\Delta J<+44$.

In order to extract the state-to-state rotational energy transfer rate constants from data similar to that shown in Fig. 4, a steady-state kinetic analysis has previously been developed.[20] The relative intensity of the satellite and parent states depends on buffer gas concentration according to

$$\frac{I(J)}{I(J_0)}=\frac{k_{RT}(J_0\rightarrow J)[M]/\Gamma_0}{1+k_Q^{\mathrm{eff}}[M]/\Gamma_0}, \quad (2)$$

where

$k_{RT}(J_0\rightarrow J)$=rate constant for rotational energy transfer from the parent state J_0 to the satellite state J,
$[M]$=concentration of the collision partner,
Γ_0= collisionless decay rate,

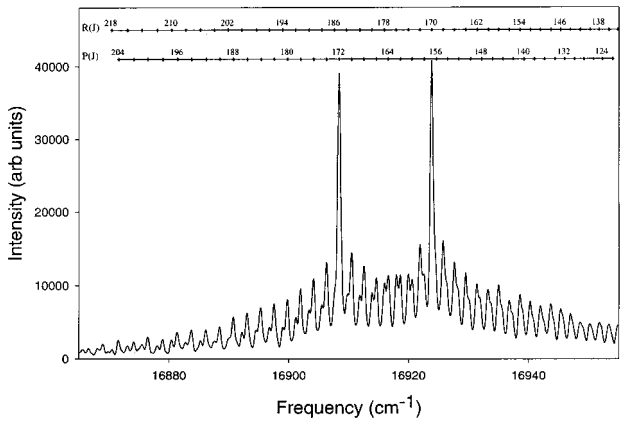

FIG. 1. Spectrally resolved $Bi_2(A-X)$ laser induced fluorescence from the $v'=1$ to $v''=5$ band in the presence of 855 m Torr of helium buffer gas after laser excitation of $v'=1$, $J=171$.

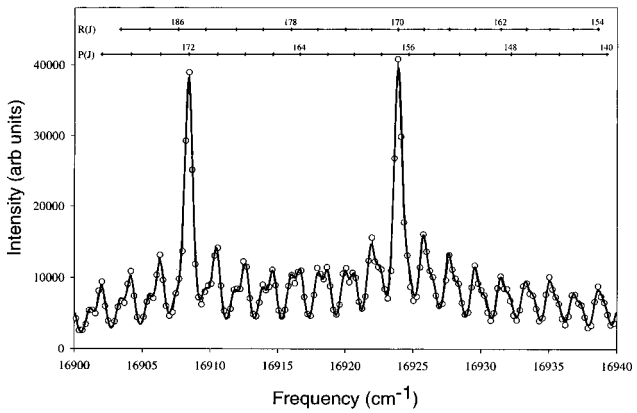

FIG. 3. Comparison of spectrally resolved Bi_2 fluorescence (○) in the presence of 855 m Torr of helium buffer gas with a spectral fit (—) to the data. The parent state of this rotational spectra is Bi_2 $(A,v'=1,J'=171)$.

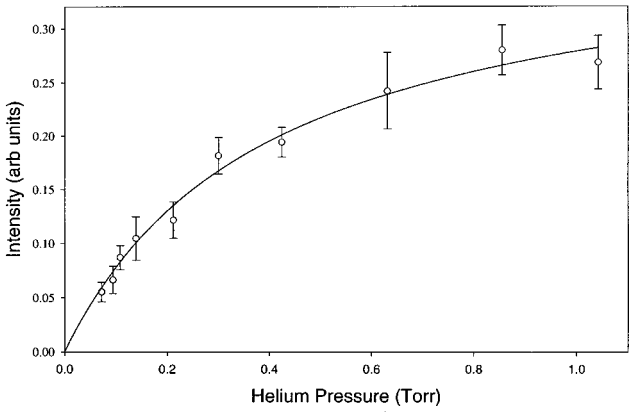

FIG. 4. Plot of the population of the satellite $J'=165$ rotational level relative to the parent state ($J'=171$) for collisions with helium buffer. The solid line is a least-squares fit to the data using Eq. (2).

k_Q^{eff}=rate constant for total removal from the rotation state J reduced by the net linear effect of multiple $R-T$ collisions.

At higher pressures the observed rotational level J can be populated by rotational energy transfer from levels other than the laser excited state. Assuming that these secondary collisions are minor and depend linearly on buffer gas concentration leads to an effective total removal rate, k_Q^{eff}. This equation has been applied successfully to rotational energy transfer in Na_2 (Ref. 21) and Br_2 (Ref. 20) and vibrational energy transfer in $Bi_2(A)$.[9] A fit of Eq. (2) to the data is also provided in Fig. 4. Using a radiative lifetime of $\tau_r=1/\Gamma_0=590\,\text{ns}$,[13] the rate constants provided in Figs. 5–7 are obtained. A tabular list of the rate constants may be found in Ref. 16. Note that no rate constants for $\Delta J=$ odd are reported in Figs. 5–7, as no intensity was observed from states of alternate parity.

IV. DISCUSSION

A. Scaling laws

Several empirical relationships have been proposed to describe the scaling of the state-to-state rotational energy transfer rate constants with rotational quantum number.[1,2] A variety of these fitting laws have been applied to the current data in an attempt to evaluate those which adequately represent the data. The exponential energy gap law (EGL) is defined by

$$k_{RT}(J_0\rightarrow J)=Af(J)e^{-c|\Delta E|/B_v}, \tag{3}$$

where

A,c=fit parameters,

$\Delta E/B_v=J(J+1)-J_0(J_0+1)$,

B_v=rotational constant,

$$f(J)=\begin{cases}\dfrac{2J_<+1}{2J_0+1} & \text{EGL1},\\ 2J+1 & \text{EGL2},\end{cases}$$

$J_<$=the smaller of J or J_0.

The statistical factor $f(J)$ depends on the distribution of final M_J levels. The EGL1 expression represents the limit where M_J is conserved and the EGL2 expression corresponds to the limit where M_J is completely randomized during a rotationally inelastic collision.

The statistical power gap law (SPG) incorporates the same two M_J statistical factors

$$k_{RT}(J_0\rightarrow J)=Bf(J)\left|\frac{\Delta E}{B_v}\right|^{-\gamma}, \tag{4}$$

where

$$f(J)=\begin{cases}\dfrac{2J_<+1}{2J_0+1}, & \text{SPG1},\\ 2J+1, & \text{SPG2},\end{cases}$$

and B and γ are the fitting parameters.

By combining the features of both the EGL and SPG fitting laws, the exponential power gap law (EPGL) is obtained

$$k_{RT}(J_0\rightarrow J)=Af(J)\left|\frac{\Delta E}{B_v}\right|^{-\gamma}e^{-c|\Delta E/B_v|}, \tag{5}$$

where

$$f(J)=\begin{cases}\dfrac{2J_<+1}{2J_0+1}, & \text{EPGL1},\\ 2J+1, & \text{EPGL2}.\end{cases}$$

Note that the EPGL has three fit parameters: A, γ, and c.

Dynamical fitting laws have also been developed, such as the infinite order sudden (IOS) and energy corrected sudden (ECS) laws. In the current work we employ an approximate version of the ECS law (ECS–P):[22]

$$\begin{aligned}k_{RT}(J_0\rightarrow J)=&A(2J+1)e^{(E_{J_0}-E_{J_>})/kT}[1+\beta^2J_>(J_>+1)]\\&\times[J_>(J_>+1)-J_<(J_<+1)]\left\{\Sigma^{2\varepsilon}F\left(\frac{\Omega}{\Sigma},\varepsilon\right)\right.\\&\left.+2\Sigma\Omega^{1+2\varepsilon}\beta^2\left[F\left(\frac{\Omega}{\Sigma},-\varepsilon\right)+\frac{\beta^2}{2}F\left(\frac{\Omega}{\Sigma},1-\varepsilon\right)\right]\right\},\end{aligned} \tag{6}$$

where

$$\beta=\frac{2B_vl_c}{\sqrt{6}\bar{v}\hbar},$$

$\bar{v}$=average relative speed of the collision pair,

l_c=interaction length fit parameter,

$J_>$=the greater of J and J_0,

$$\Sigma=\sqrt{B_vJ_>(J_>+1)}+\sqrt{B_vJ_<(J_<+1)},$$

$$\Omega=\sqrt{B_vJ_>(J_>+1)}-\sqrt{B_vJ_<(J_<+1)},$$

$$F(x,z)=h(z)+[1-h(z)]x^{[1+g(z)]},$$

$$h(z)=\frac{1}{\sqrt{\pi}}\frac{\Gamma(z+1/2)}{\Gamma(z+1)},$$

Γ=gamma function,

$$g(z)=\begin{cases}z, & z\geqslant 0,\\ 2z-0.05, & z<0.\end{cases}$$

The ECS–P law also has three fit parameters, A, β, and ε.

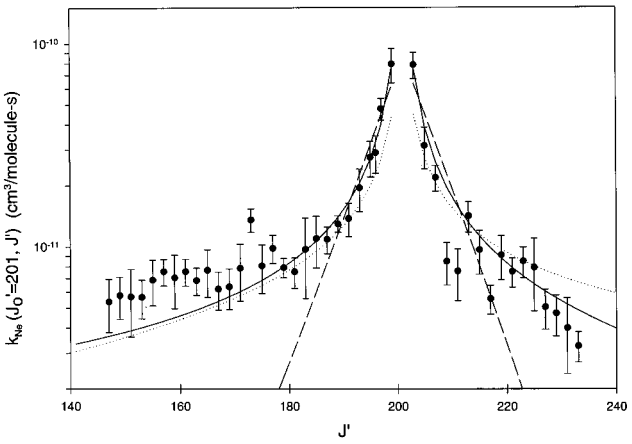

FIG. 5. State-to-state rotational energy transfer rate constants for Ne after laser excitation of $v'=1$, $J'=201$. Three scaling law fits are also shown (—) SPG1, (···) SPG2, and (---) EGL1.

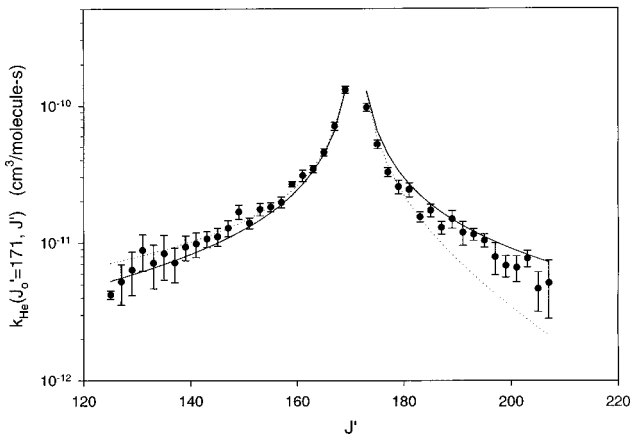

FIG. 7. State-to-state rotational energy transfer rate constants for He after laser excitation of $v'=1$, $J'=171$. Two scaling law fits are also shown (—) SPG1 and (···) ECS–P.

In Fig. 5, a fit of the SPG1, SPG2, and EGL1 fitting laws are shown. The exponential gap law fails for all the initially prepared J_0 levels and buffer gas studies observed in the present work. The EGL1 and EGL2 fitting laws can be made to represent either the rotational levels near the pumped state, or for larger ΔJ, but not both. The statistical power gap laws do provide an adequate representation of the data for all J_0 and all three collision partners. The M_J conserving form of the statistical factor $f(J)$ (SPG1) provides a fit standard error of 20–50 % less than the completely randomized factor (SPG2) and in all cases provides a better fit.

Figure 6 illustrates the rate constants for helium collisions after laser excitation of $J_0=201$. While the EPGL law provides a slightly improved fit over the SPG fits, the exponential fit parameter, c, is poorly determined and yields a near zero value. Furthermore the F statistic for the EPGL1 fits is about one-half of the value for the SPG1 fits. The addition of the third parameter to capture any exponential type behavior is not warranted.

Finally, a comparison of the ECS–P and SPG1 fitting laws is provided in Fig. 7. The standard errors for the ECS–P law are larger than for the SPG1 law, despite the addition of a third fitting parameter. In addition, the ECS–P fit parameters yield large values for the interaction length, l_c. In summary, the statistical power gap law of Eq. (4), particularly with the statistical factor associated with M_J conserving collisions, provides superior fits for the present data. Fit parameters for the statistical power gap law (SPG1) are summarized for each of the collision partners in Table II.

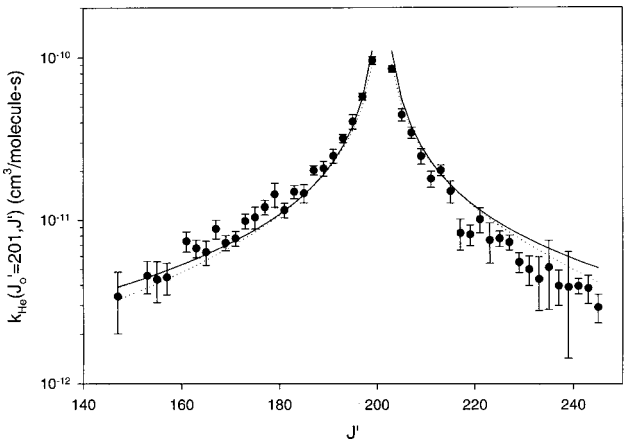

FIG. 6. State-to-state rotational energy transfer rate constants for He after laser excitation of $v'=1$, $J'=201$. Two scaling law fits are also shown (—) SPG1 and (···) EPGL1.

A systematic deviation from the statistical power gap law is observed for the heavier collision partners, Ne and Ar, at large ΔJ. Figure 8 summarizes all the state-to-state rotational energy transfer rates after laser excitation of $J_0'=201$ as observed in this study. The SPG1 scaling law should provide a nearly linear relationship on this logarithmic plot. [For a statistical factor $f(J)=1$, the plot would provide a constant slope.] The helium data is well represented by the linear relationship. However, for $\Delta E \geqslant 300\,\mathrm{cm}^{-1}$, the Ar and He rates are larger than expected. It is possible that the high ΔJ rates are overestimated by neglecting the full effects of multiple collisions. On the other hand, the statistical power gap law may fail for large ΔJ and heavier collision partners.

A key assumption of the statistically based scaling laws is that the transition probabilities depend only on the energy difference, not on the initial rotational state.[1] A simultaneous fit of Eq. (4) to the helium data for $J_0=171$, 201, and 231 provides average values of $B=4.0\pm0.5\times10^{-8}\,\mathrm{cm}^3/\mathrm{molecule\,s}$ and $\gamma=0.898\pm0.018$. However, there is a definite dependence of the SPG1 fit parameters on initial rotational level, J_0, for the helium data in Table II. As the initial rotational levels increases, the width of the distribution increases (γ decreases) and there is a corresponding decrease in the amplitude, B. Similar results have been observed for other molecule–atom systems.[1] The fitting laws

TABLE II. Fit parameters for the statistical power gap scaling law, SPG1.

Collision partner	(v',J_0')	B (10^{-8} cm^3/molecule s)	γ
He	(1,171)	5.45±1.17	0.944±0.030
He	(1,201)	3.85±0.59	0.902±0.021
He	(1,231)	2.79±0.50	0.834±0.025
Ne	(1,201)	5.00±1.23	0.968±0.034
Ar	(1,201)	1.25±0.50	0.786±0.042

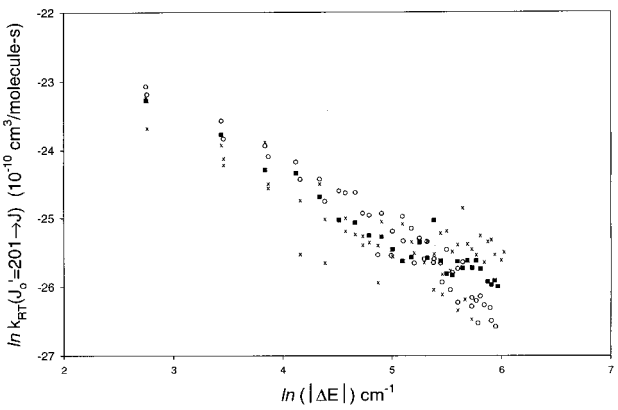

FIG. 8. Observed rotation energy transfer rate constants from $J_0'=201$ as a function of change in rotation energy: (○) He, (■) Ne, and (×) Ar.

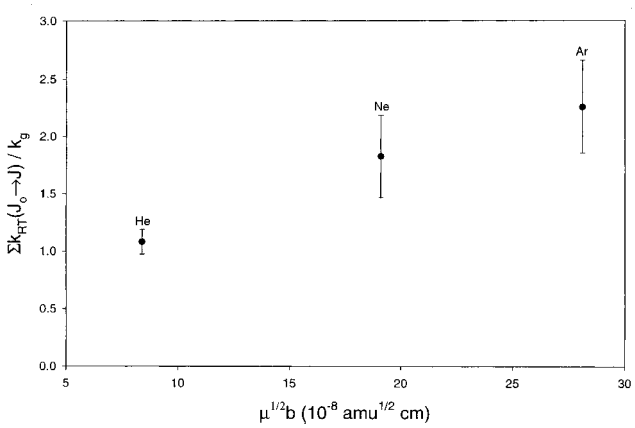

FIG. 9. Probability for total rotational removal depends on total angular momentum available, as expressed in Eq. (7).

are empirical and a clear physical interpretation of the fit parameters is difficult.

B. Total removal rates

The total rotational removal rates, $\Sigma_{J=0}^{\infty}k_{RT}(J_0\rightarrow J)$, are summarized in Table III. Gas kinetic collision rate constants, k_g, are also provided as estimated from the collision radii.[23] Rotational energy transfer within $Bi_2(A)$ is rapid, with the total rotational removal within a factor of 3 of the gas kinetic rates. These results compare favorably with the previously measured argon total quenching rates for $v'=1$ of $2.4\times10^{-10}\,\mathrm{cm}^3/\mathrm{molecule\,s}$.[14] The probability for rotational energy transfer, as described by the ratio of the observed total removal rates to the gas kinetic rates increases linearly with angular momentum,[7]

$$L=\mu\bar{v}b=\sqrt{\frac{8kT}{\pi}}\mu^{1/2}b \tag{7}$$

as show in Fig. 9. In this figure the impact parameter, b, is chosen to be the sum of the particle radii.[23] On average, the heavier collision partners bring more orbital angular momentum into the collision.

There are fewer rotational levels accessible for a given ΔE at higher initial rotational states, J_0. As a result, the total rotational removal rates also decrease with increasing J_0. Other previous studies have observed similar trends.[1,7,20]

The effective quenching rates constants, k_Q^{eff}, as defined by the fits of Eq. (2), yield values of $3.0-0.2\times10^{-10}\,\mathrm{cm}^3/\mathrm{molecule\,s}$, depending on J.[18] These rates are slower than the total rotational removal rates, due to multiple $R-T$ collisions as discussed for Eq. (2).

TABLE III. Total rotational removal rates ($10^{-10}\,\mathrm{cm}^3/\mathrm{molecule\,s}$).

Collision partner	J_0'	k_g	$\Sigma k_{RT}(J_0\rightarrow J)$
He	171	7.0	8.9
He	201	7.0	7.6
He	231	7.0	6.9
Ne	201	3.4	6.2
Ar	201	2.8	6.4

V. CONCLUSION

Rotational energy transfer within $Bi_2(A)$ is rapid, constrained to $\Delta J=$even by parity conservation, and best represented by the statistical power gap scaling law with M_J conservation. Single collision population of rotational levels with $|\Delta J|\leqslant52$, $\Delta E>300\,\mathrm{cm}^{-1}$, is readily apparent. Even for these very high rotational states, with large angular momentum, the energy based scaling laws appear to provide a better representation of the rates than the energy corrected sudden with a power law for the angular momentum scaling.

[1] T. A. Brunner and D. Pritchard, "Fitting laws for rotationally inelastic collisions" in *Advances in Chemical Physics, Volume 50: Dynamics of the Excited State*, edited by K. P. Lawley (Wiley, New York, 1982).
[2] J. I. Steinfeld, P. Ruttenberg, G. Millot, G. Fanjoux, and B. Lavorel, J. Phys. Chem. **95**, 9638 (1991).
[3] J. T. Yardley, *Introduction to Molecular Energy Transfer* (Academic, New York, 1980).
[4] J. I. Steinfeld, J. Phys. Chem. Ref. Data **13**, 445 (1984).
[5] A. J. McCaffrey, Z. T. Alwahabi, M. A. Osborne, and C. J. Williams, J. Chem. Phys. **98**, 4586 (1993).
[6] *Atom–Molecule Collision Theory*, edited by R. B. Bernstein (Plenum, New York, 1979).
[7] A. Schiffman and D. W. Chandler, Int. Rev. Phys. Chem. **14**, 371 (1995).
[8] P. J. Dagdigian, *The Chemical Dynamics and Kinetics of Small Radicals* (World Scientific, Singapore, 1995).
[9] R. E. Franklin and G. P. Perram, J. Chem. Phys. **111**, 5757 (1999).
[10] R. F. Barrow, F. Taher, J. D. Incani, C. Effantin, A. J. Ross, A. Topovzkhanian, G. Wannous, and J. Verges, Mol. Phys. **87**, 725 (1996).
[11] R. E. Franklin and G. P. Perram, J. Mol. Spectrosc. **194**, 1 (1999).
[12] G. Gerber, Honinger, and J. James, Chem. Phys. Lett. **85**, 415 (1982).
[13] J. M. Blondeau, G. Gandara, P. Carette, and J. Messelyn, Chem. Phys. Lett. **71**, 246 (1980).
[14] G. Ehret and G. Gerber, Chem. Phys. **66**, 27 (1982).
[15] M. W. Dolezal, Ph.D. dissertation, Air Force Institute of Technology, AFIT/DS/ENP/01-01, 2001.
[16] W. P. West and H. P. Broida, Chem. Phys. Lett. **56**, 283 (1978).
[17] S. Drosch and G. Gerber, J. Chem. Phys. **77**, 123 (1982).
[18] R. E. Franklin, Ph.D. dissertation, Air Force Institute of Technology, AFIT/DS/ENP/97-04, 1997.
[19] C. W. McCurdy and W. H. Miller, J. Chem. Phys. **67**, 463 (1977).
[20] G. P. Perram, D. A. Massman, and S. J. Davis, J. Chem. Phys. **99**, 6634 (1993).
[21] K. Bergmann and W. Demtröder, Z. Phys. **243**, 1 (1971).
[22] N. Smith and D. E. Pritchard, J. Chem. Phys. **74**, 3939 (1981).
[23] J. O. Hirschfelder, C. F. Curtis, and R. B. Byrd, *Molecular Theory of Gases and Liquids* (Wiley, New York, 1954).